



Cite this: *CrystEngComm*, 2015, 17, 6320

## Pillared-bilayer zinc(II)–organic laminae: pore modification and selective gas adsorption†

Li-Wei Lee,<sup>ab</sup> Tzuoo-Tsair Luo,<sup>a</sup> Sheng-Han Lo,<sup>a</sup> Gene-Hsiang Lee,<sup>d</sup> Shie-Ming Peng,<sup>d</sup> Yen-Hsiang Liu,<sup>\*c</sup> Sheng-Long Lee<sup>\*b</sup> and Kuang-Lieh Lu<sup>\*a</sup>

Three porous metal–organic frameworks, namely  $\{[\text{Zn}_2(\text{azpy})(\text{aip})_2] \cdot 2\text{DMF}\}_n$  (**1**, azpy = 4,4'-azobipyridine,  $\text{H}_2\text{aip}$  = 5-aminoisophthalic acid),  $\{[\text{Zn}_2(\text{dipyzt})(\text{aip})_2] \cdot 1.15\text{DMF} \cdot 0.85\text{MeOH}\}_n$  (**2**, dipyzt = di-3,6-(4-pyridyl)-1,2,4,5-tetrazine) and  $\{[\text{Zn}_2(\text{tpim})(\text{aip})_2] \cdot 2.5\text{DMF} \cdot 2\text{H}_2\text{O}\}_n$  (**3**, tpim = 2,4,5-tri(4-pyridyl)imidazole), were synthesized under mild conditions. All of the compounds consisted of a honeycomb-like layer,  $[\text{Zn}(\text{aip})]_n$ , further pillared by N-donor ligands to form two-dimensional (2D) porous pillared-bilayer frameworks with 1D channels created inside the bilayers ( $4.1 \times 10.1 \text{ \AA}^2$  for **1**,  $4.1 \times 11.1 \text{ \AA}^2$  for **2**, and  $5.1 \times 9.8 \text{ \AA}^2$  for **3**). The resulting MOFs showed different pore volumes and channel shapes depending on the length and shape of the pillar ligands (35.7%, 41.7%, and 33.9% for **1–3**, respectively). The pore volume in **3** decreased due to the presence of the uncoordinated pyridyl group of the tpim ligand. The frameworks of **1** and **2** show flexible properties upon undergoing solvent-exchange processes and their  $\text{CO}_2$  adsorption properties are different. These latter properties are affected by the functional groups of the linear pillar ligand ( $-\text{N}=\text{N}-$  and tetrazine group). In particular, compound **3** possesses less flexibility upon undergoing a solvent-exchange process and preferentially absorbs  $\text{CO}_2$  more efficiently rather than  $\text{H}_2$  and  $\text{N}_2$ .

Received 12th May 2015,  
Accepted 9th July 2015

DOI: 10.1039/c5ce00923e

www.rsc.org/crystengcomm

## Introduction

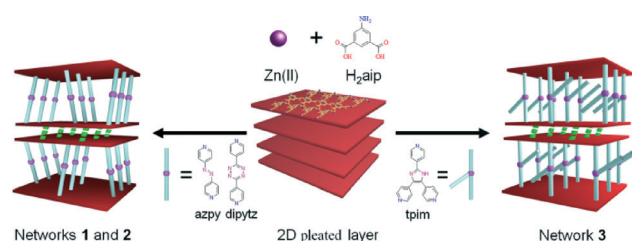
Metal–organic frameworks (MOFs) have attracted considerable attention, not only due to their intriguing structural topologies,<sup>1</sup> but also because of their designable properties and potential applications in gas storage/separation,<sup>2</sup> catalysis,<sup>3</sup> sensing,<sup>4</sup> etc. Employing rational design strategies in the construction of porous MOFs with high surface areas, predictable structures, tunable pore sizes, and functionality has been among the most compelling challenges to date. In particular, pillared-bilayer porous MOFs are very rare in comparison with many published pillared-layer structures mainly due to the lack of a systematic synthetic strategy.<sup>5</sup> We envisaged that a tetrahedral metal centre, *i.e.*  $\text{Zn}^{2+}$ , in combination with tridentate ligands might produce a layered structure with a vacant site in each metal centre. Followed by the coordination of a ditopic functional ligand as a pillar linker, this may result in the formation of pillared-bilayer MOFs in reasonable yield.<sup>6</sup> Herein, we report the successful preparation of three  $\text{Zn}(\text{II})$ -

based pillared-bilayer MOFs by following this synthetic method (Scheme 1). In addition, by introducing pillar ligands with different sizes, shapes and functional groups, the pore size and flexibility of the pillared-bilayer structures can be tuned.<sup>7</sup> These unusual structural characteristics allow the pillared-bilayer MOFs to serve as excellent models for studies of gas adsorption properties.

## Experimental section

### Materials and general methods

All reagents and solvents were purchased from commercial sources and used as-received without further purification. 4,4'-Azobipyridine (azpy),<sup>8</sup> di-3,6-(4-pyridyl)-1,2,4,5-tetrazine (dipyzt)<sup>9</sup> and 2,4,5-tri(4-pyridyl)imidazole (tpim)<sup>10</sup> were prepared according to literature methods. Infrared spectra were recorded from KBr pellets in the  $4000\text{--}400 \text{ cm}^{-1}$  range on a



**Scheme 1** Design and synthesis of the pillared-bilayer frameworks **1–3**.

<sup>a</sup> Institute of Chemistry, Academia Sinica, Taipei 115, Taiwan.  
E-mail: kllu@gate.sinica.edu.tw; Tel: +886 2 27898518

<sup>b</sup> Institute of Materials Science and Engineering, National Central University, Taoyuan 320, Taiwan

<sup>c</sup> Department of Chemistry, Fu Jen Catholic University, Taipei 242, Taiwan

<sup>d</sup> Department of Chemistry, National Taiwan University, Taipei 107, Taiwan

† Electronic supplementary information (ESI) available: Additional figures for the crystal structures, TGA spectra, FTIR spectra, PXRD patterns and Fig. S1–S21. CCDC 1063484–1063486. See DOI: 10.1039/c5ce00923e

Perkin-Elmer Paragon 1000 FT-IR spectrometer. Elemental analyses were performed using a Perkin-Elmer 2400 CHN elemental analyzer. Thermogravimetric analysis (TGA) was performed under nitrogen with a Perkin-Elmer TGA-7 TG analyzer. Powder X-ray diffraction (PXRD) measurements were recorded on an MPD Philips analytical diffractometer at 40 kV and 30 mA with Cu K $\alpha$  radiation ( $\lambda$  = 1.5406 Å). Brunauer-Emmett-Teller (BET) analyses were carried out with a Micromeritics ASAP 2020 system using nitrogen and hydrogen as adsorbates at 77 K and carbon dioxide at 195 K, 273 K and 298 K.

**Synthesis of  $\{[\text{Zn}_2(\text{azpy})(\text{aip})_2]\cdot 2\text{DMF}\}_n$  (1).** A mixture of  $\text{Zn}(\text{NO}_3)_2\cdot 6\text{H}_2\text{O}$  (30.1 mg, 0.101 mmol), azpy (9.2 mg, 0.05 mmol), and  $\text{H}_2\text{aip}$  (18.1 mg, 0.101 mmol) was dissolved in a solution of dimethylformamide (DMF, 7 mL) and  $\text{H}_2\text{O}$  (1 mL). The mixture was sealed in a glass vial and heated at 50 °C in a water bath for 4 days. Plate-shaped orange crystals of **1** were isolated by filtration, washed with water and ethanol, and dried in air. Yield: 44% (18.9 mg, based on azpy). FT-IR (KBr pellet,  $\text{cm}^{-1}$ ): 3482 (m), 3253 (m), 3140 (m), 1678 (s), 1625 (s), 1574 (s), 1478 (m), 1441 (m), 1386 (s), 1343 (s), 1248 (m), 1132 (m), 1098 (m), 961 (m), 932 (w), 852 (m), 797 (m), 777 (m), 731 (m), 678 (w), 604 (w), 571 (w), 530 (w). Elemental analysis calcd (%) for  $\text{C}_{16}\text{H}_{18}\text{N}_4\text{ZnO}_6$ : C, 44.92; H, 4.24; N, 13.09; found: C, 45.05; H, 4.22; N, 13.21. The formula  $[\text{Zn}_2(\text{azpy})(\text{aip})_2]\cdot 2\text{DMF}\cdot 2\text{H}_2\text{O}$  was assigned based on elemental analysis and thermogravimetric analysis.

**Synthesis of  $\{[\text{Zn}_2(\text{dipyzt})(\text{aip})_2]\cdot 1.15\text{DMF}\cdot 0.85\text{MeOH}\}_n$  (2).** A mixture of  $\text{Zn}(\text{NO}_3)_2\cdot 6\text{H}_2\text{O}$  (30.1 mg, 0.101 mmol), dipyzt (11.7 mg, 0.051 mmol), and  $\text{H}_2\text{aip}$  (18.2 mg, 0.101 mmol) was dissolved in a solution of DMF (7 mL), MeOH (1 mL) and EtOH (1 mL). The mixture was sealed in a glass vial and heated at 50 °C in a water bath for 4 days. Plate-shaped red crystals of **2** were isolated by filtration, washed with water and ethanol, and dried in air. Yield: 54% (22.7 mg, based on dipyzt). FT-IR (KBr pellets,  $\text{cm}^{-1}$ ): 3438 (m), 3254 (m), 3140 (m), 1667 (s), 1627 (s), 1574 (s), 1478 (m), 1441 (m), 1384 (s), 1342 (s), 1248 (m), 1133 (m), 1099 (m), 961 (m), 927 (w), 795 (m), 777 (m), 731 (m), 685 (w), 604 (w), 571 (w), 536 (w). Elemental analysis calcd (%) for  $\text{C}_{32.3}\text{H}_{33.45}\text{N}_{9.15}\text{Zn}_2\text{O}_{12}$ : C, 44.45; H, 3.86; N, 14.69; found: C, 44.16; H, 4.01; N, 14.82. The formula  $[\text{Zn}_2(\text{dipyzt})(\text{aip})_2]\cdot 1.15\text{DMF}\cdot 0.85\text{MeOH}\cdot 2\text{H}_2\text{O}$  was assigned based on elemental analysis and thermogravimetric analysis.

**Synthesis of  $\{[\text{Zn}_2(\text{tpim})(\text{aip})_2]\cdot 2.5\text{DMF}\cdot 2\text{H}_2\text{O}\}_n$  (3).** A mixture of  $\text{Zn}(\text{NO}_3)_2\cdot 6\text{H}_2\text{O}$  (29.9 mg, 0.099 mmol), tpim (14.9 mg, 0.049 mmol), and  $\text{H}_2\text{aip}$  (18.1 mg, 0.101 mmol) was dissolved in a solution of DMF (7 mL),  $\text{H}_2\text{O}$  (1 mL), MeOH (1 mL) and EtOH (1 mL). The mixture was sealed in a glass vial and heated at 50 °C in a water bath for 4 days. Plate-shaped colorless crystals of **3** were isolated by filtration, washed with water and ethanol, and dried in air. Yield: 79% (39.8 mg, based on tpim). FT-IR (KBr pellets,  $\text{cm}^{-1}$ ): 3454 (m), 3262 (m), 3143 (m), 1668 (s), 1621 (s), 1574 (s), 1479 (m), 1441 (m), 1386 (s), 1346 (s), 1133 (m), 1098 (m), 1028 (m), 963 (m), 847 (w), 833 (w), 796 (m), 779 (m), 731 (m), 680 (w), 663 (w), 612

(w), 562 (w), 530 (w), 512 (w). Elemental analysis calcd (%) for  $\text{C}_{41.5}\text{H}_{45.5}\text{N}_{9.5}\text{Zn}_2\text{O}_{12.5}$ : C, 49.49; H, 4.45; N, 13.21; found: C, 49.06; H, 4.35; N, 13.13.

### Single-crystal structure analyses

Diffraction measurements for compounds **1–3** were carried out using a Bruker SMART APEX CCD diffractometer with graphite-monochromated Mo K $\alpha$  radiation ( $\lambda$  = 0.71073 Å). The crystal structures were solved with direct methods and refined using the SHELXL-97 (ref. 11) program by full-matrix least-squares on  $F^2$  values. The positions of the C–H hydrogen atoms were generated geometrically and the isotropic thermal parameters were assigned. In **2**, the disordered pyridyl ring of the dipytz ligand was modeled over two occupied sites with refined site occupancy factors of 0.823 (C12A and C13A) and 0.177 (C12B and C13B). Isotropic restraints (ISOR) were applied to DMF and methanol solvents and the atoms of N1, N3, N4, C11 and C14. In **3**, the imidazole and pyridyl rings of the tpim ligand were disordered with a 50% site occupancy (Fig. S9†). However, the hydrogen atoms of the lattice water molecule in **3** could not be positioned reliably. Isotropic restraints (ISOR) were applied to water solvents (O10 and O11). Crystal data and structure refinement results for **1–3** are listed in Table 1, and the selected bond lengths and angles are given in Table 2.

## Results and discussion

### Syntheses of **1–3**

The reaction of  $\text{Zn}(\text{NO}_3)_2\cdot 6\text{H}_2\text{O}$ , 5-aminoisophthalic acid ( $\text{H}_2\text{aip}$ ) and the pillar ligands, 4,4'-azobipyridine (azpy), di-3,6-(4-pyridyl)-1,2,4,5-tetrazine (dipyzt), or 2,4,5-tri(4-pyridyl)imidazole (tpim), in a 2 : 2 : 1 molar ratio at 50 °C for four days resulted in the formation of three Zn(II)-based pillared-bilayer frameworks, namely  $\{[\text{Zn}_2(\text{azpy})(\text{aip})_2]\cdot 2\text{DMF}\}_n$  (**1**),  $\{[\text{Zn}_2(\text{dipyzt})(\text{aip})_2]\cdot 1.15\text{DMF}\cdot 0.85\text{MeOH}\}_n$  (**2**), and  $\{[\text{Zn}_2(\text{tpim})(\text{aip})_2]\cdot 2.5\text{DMF}\cdot 2\text{H}_2\text{O}\}_n$  (**3**), as highly crystalline products (Scheme 1).

### Description of the crystal structures

**Crystal structures of  $\{[\text{Zn}_2(\text{azpy})(\text{aip})_2]\cdot 2\text{DMF}\}_n$  (1),  $\{[\text{Zn}_2(\text{dipyzt})(\text{aip})_2]\cdot 1.15\text{DMF}\cdot 0.85\text{MeOH}\}_n$  (2), and  $\{[\text{Zn}_2(\text{tpim})(\text{aip})_2]\cdot 2.5\text{DMF}\cdot 2\text{H}_2\text{O}\}_n$  (3).** Single-crystal X-ray diffraction analyses revealed that compounds **1** and **2** crystallize in the monoclinic space group  $P2_1/c$ . The asymmetric unit of **1** contains one  $\text{Zn}^{\text{II}}$  ion, one-half of an azpy ligand, one  $\text{aip}^{2-}$  ligand, and one guest DMF molecule. The centre of the  $\text{N}=\text{N}$  double bond of the azpy ligand is located about a crystallographic inversion centre. On the other hand, the guest DMF molecule is unequally disordered over two sites. Each  $\text{Zn}^{\text{II}}$  centre is coordinated to one pyridyl nitrogen atom of the azpy ligand, one amino nitrogen atom of the  $\text{aip}^{2-}$  ligand, and two monodentate carboxylate oxygen atoms from two different  $\text{aip}^{2-}$  ligands in a distorted tetrahedral geometry (Fig. 1a). As shown in Fig. 1b, each  $\text{aip}^{2-}$  ligand is bound to

**Table 1** Summary of crystal data and structure refinement for 1–3

Compound	1	2	3
Empirical formula	C <sub>16</sub> H <sub>16</sub> N <sub>4</sub> O <sub>5</sub> Zn	C <sub>32.3</sub> H <sub>29.45</sub> N <sub>9.15</sub> O <sub>10</sub> Zn <sub>2</sub>	C <sub>41.5</sub> H <sub>44.5</sub> N <sub>9.5</sub> O <sub>12.5</sub> Zn <sub>2</sub>
<i>F</i> <sub>w</sub>	409.70	836.54	1007.11
Crystal system	Monoclinic	Monoclinic	Monoclinic
Space group	<i>P</i> 2 <sub>1</sub> / <i>c</i>	<i>P</i> 2 <sub>1</sub> / <i>c</i>	<i>P</i> 2 <sub>1</sub> / <i>n</i>
<i>a</i> , Å	14.521(3)	16.9909(15)	16.0364(6)
<i>b</i> , Å	7.7378(15)	7.6688(7)	7.6528(3)
<i>c</i> , Å	15.997(3)	16.0077(15)	35.3947(14)
<i>α</i> /°	90	90	90
<i>β</i> /°	106.40(3)	102.322(2)	99.7638(13)
<i>γ</i> /°	90	90	90
<i>V</i> /Å <sup>3</sup>	1724.3(6)	2037.8(3)	4280.8(3)
<i>Z</i>	4	2	4
<i>λ</i> /Å	0.71073	0.71073	0.71073
<i>D</i> <sub>calc</sub> /g cm <sup>−3</sup>	1.578	1.363	1.563
<i>μ</i> /mm <sup>−1</sup>	1.460	1.238	1.198
<i>F</i> (000)	840	855	2080
GOF	1.079	1.136	1.022
<i>R</i> <sub>1</sub> <sup>a</sup> , <i>wR</i> <sub>2</sub> <sup>b</sup> [ <i>I</i> > 2σ( <i>I</i> )]	0.0424, 0.0988	0.0851, 0.2369	0.0518, 0.1497
<i>R</i> <sub>1</sub> <sup>a</sup> , <i>wR</i> <sub>2</sub> <sup>b</sup> (all data)	0.0535, 0.1034	0.1240, 0.2651	0.0852, 0.1744

$$^a R_1 = \sum ||F_o| - |F_c|| / \sum |F_o|, \quad ^b wR_2 = \{ \sum [w(F_o^2 - F_c^2)^2] / \sum [w(F_o^2)^2] \}^{1/2}.$$

**Table 2** Selected bond lengths (Å) and angles (°) for 1–3

<b>1</b>			
Zn(1)–O(1)	1.942(2)	Zn(1)–O(3)#4	1.993(2)
Zn(1)–N(1)#5	2.058(3)	Zn(1)–N(2)	2.02(2)
O(1)–Zn(1)–O(3)#4	102.47(8)	O(1)–Zn(1)–N(1)#5	112.75(10)
O(3)#4–Zn(1)–N(2)	122.3(3)	O(1)–Zn(1)–N(2)	103.4(5)
N(2)–Zn(1)–N(1)#5	108.0(2)	O(3)#4–Zn(1)–N(1)#5	107.84(10)
<b>2</b>			
Zn(1)–O(1)	1.938(5)	Zn(1)–O(3)#1	1.995(6)
Zn(1)–N(2)	2.029(7)	Zn(1)–N(1)#2	2.057(7)
O(1)–Zn(1)–O(3)#1	100.5(2)	O(1)–Zn(1)–N(1)#2	114.3(3)
O(1)–Zn(1)–N(2)	101.4(3)	O(3)#1–Zn(1)–N(1)#2	106.7(3)
O(3)#1–Zn(1)–N(2)	123.9(3)	N(2)–Zn(1)–N(1)#2	109.9(3)
<b>3</b>			
Zn(1)–O(7)	1.943(3)	Zn(2)–O(3)	1.940(3)
Zn(1)–O(1)	1.983(3)	Zn(2)–O(6)#3	2.000(3)
Zn(1)–N(5)	2.038(4)	Zn(2)–N(2)#4	2.055(4)
Zn(1)–N(1)#1	2.052(4)	Zn(2)–N(6)#2	2.103(13)
O(7)–Zn(1)–O(1)	100.09(12)	O(3)–Zn(2)–O(6)#3	99.86(12)
O(7)–Zn(1)–N(5)	99.83(14)	O(3)–Zn(2)–N(2)#4	117.78(14)
O(1)–Zn(1)–N(5)	123.46(14)	O(6)#3–Zn(2)–N(6)#2	117.5(3)
O(7)–Zn(1)–N(1)#1	109.63(14)	O(6)#3–Zn(2)–N(2)#4	104.50(14)
O(1)–Zn(1)–N(1)#1	107.42(14)	O(3)–Zn(2)–N(6)#2	106.5(3)
N(5)–Zn(1)–N(1)#1	114.40(16)	N(2)#4–Zn(2)–N(6)#2	110.8(4)

Symmetry transformations used to generate equivalent atoms: for 1: #4 *x*, −*y* + 3/2, *z* + 1/2; #5 *x*, −*y* + 1/2, *z* + 1/2; for 2: #1 *x*, −*y* + 5/2, *z* − 1/2; #2 *x*, −*y* + 3/2, *z* − 1/2; for 3: #1 *x*, *y* − 1, *z*; #2 −*x* + 2, −*y* + 1, −*z*; #3 *x* + 1, *y*, *z*; #4 *x* + 1, *y* + 1, *z*.

three different Zn<sup>II</sup> ions by two monodentate carboxylate groups and one amino group [Zn<sup>II</sup>⋯Zn<sup>II</sup> separation of 7.74(16)–8.90(15) Å] (Fig. S1†). Thus, each Zn<sup>II</sup> ion is surrounded by three bridging aip<sup>2−</sup> ligands to form a pleated (6,3) honeycomb-like layer with aperture dimensions of 3.4 × 4.9 Å<sup>2</sup> (Fig. S2†). In addition, the Zn<sup>II</sup> ion is further connected to one pillar linker azpy in a tetrahedral fashion, leading to the formation of a pillared-bilayer structure (Fig. 1c). The

Zn<sup>II</sup>⋯Zn<sup>II</sup> distance across the azpy bridge is 13.1(30) Å. It is significant that large square-shaped channels were observed within the framework along the *b* axis with effective dimensions of 4.1 × 10.1 Å<sup>2</sup> (Fig. 1d). Smaller channels were also observed along the *c* axis with dimensions of 3.1 × 4.3 Å<sup>2</sup> (Fig. S3a†). Analysis using PLATON (ref. 12) software indicated that the extra-framework volume per unit cell is approximately 35.7%.

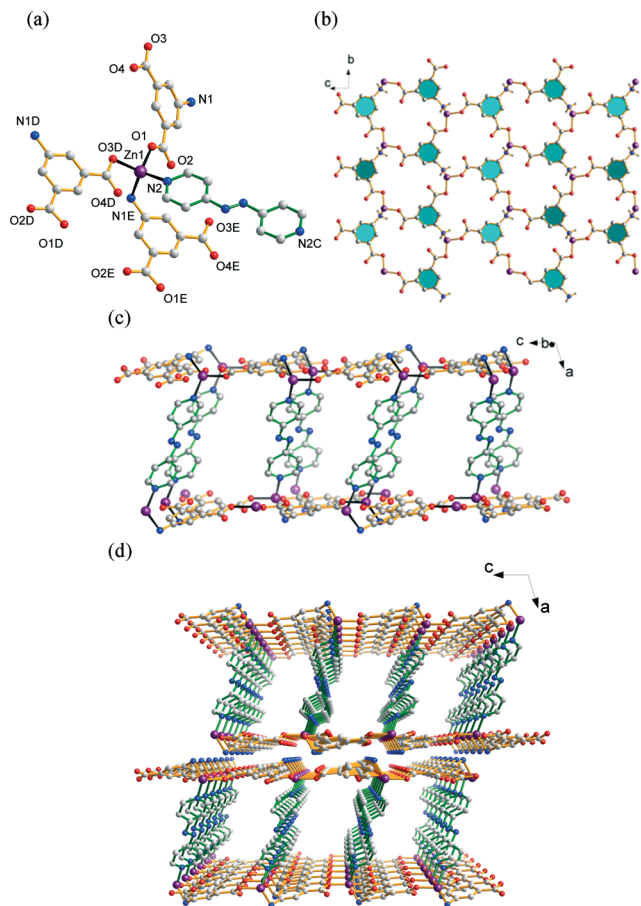


**Fig. 1** (a) Coordination environments of the  $\text{Zn}^{\text{II}}$  ion in **1**. (b) A perspective view of the pleated layer in **1**. (c) 2D pillared-bilayer network of **1** along the  $b$  axis. (d) The pillared-bilayer network of **1** showing large 1D channels observed along the  $b$  axis. Symmetry transformations used to generate equivalent atoms: (C)  $-x + 1, -y, -z + 1$ ; (D)  $x, -y + 3/2, z + 1/2$ ; (E)  $x, -y + 1/2, z + 1/2$ .

Compounds **1** and **2** differ from one another based on only the pillar linkers and lattice guest molecule. The asymmetric unit of **2** contains one  $\text{Zn}^{\text{II}}$  ion, one-half of a dipytz ligand, one  $\text{aip}^{2-}$  ligand, one-half of a guest DMF molecule, and half of a guest MeOH molecule. The centre of the dipytz ligand is located about a crystallographic inversion centre. The guest DMF molecule is in a general position with the site occupancy factor refined to be 0.575. In addition, the guest methanol molecule is in a general position with the site occupancy factor refined to be 0.425. The  $\text{Zn}^{\text{II}}$  centre adopts the same distorted tetrahedral coordination environment as that in **1** (Fig. 2a). The layers in compound **2** have the same coordination mode as that in **1**, while the bond distances changed because the azpy ligand is replaced with the dipytz ligand. As a consequence, the dipytz ligand acts as a pillar to support the infinite 2D layers, thus leading to an extended 2D pillared-bilayer structure with a  $\text{Zn} \cdots \text{Zn}$  separation distance of  $15.1(18) \text{ \AA}$  (Fig. 2b). Large square-shaped channels were observed within the framework along the  $b$  axis with effective dimensions of  $4.1 \times 11.1 \text{ \AA}^2$  and smaller channels

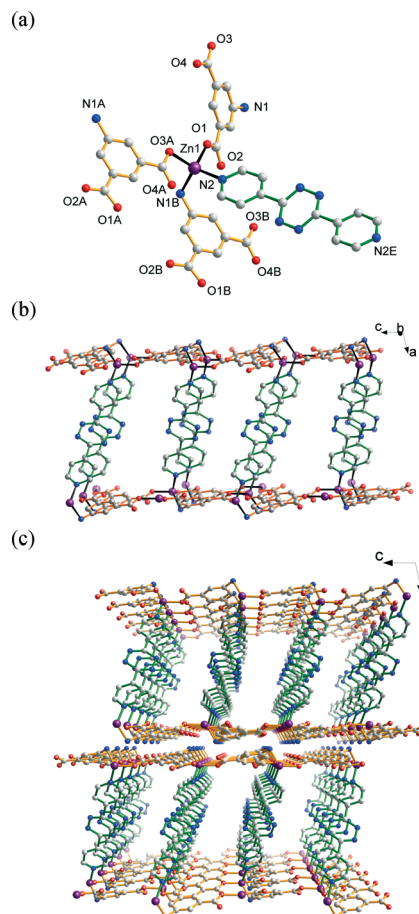
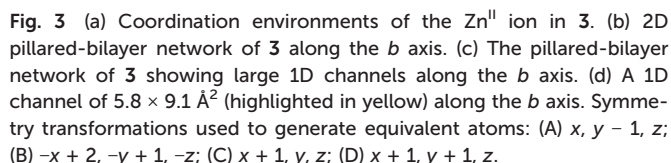


**Fig. 2** (a) Coordination environments of the  $\text{Zn}^{\text{II}}$  ion in **2**. (b) 2D pillared-bilayer network of **2** along the  $b$  axis. (c) Pillared-bilayer network of **2** showing large 1D channels along the  $b$  axis. Symmetry transformations used to generate equivalent atoms: (A)  $x, -y + 5/2, z - 1/2$ ; (B)  $x, -y + 3/2, z - 1/2$ ; (E)  $-x + 1, -y + 1, -z$ .

were also observed along the  $c$  axis with dimensions of  $4.3 \times 4.4 \text{ \AA}^2$  (Fig. 2c and S4a†). Analysis using PLATON software indicated that the extra-framework volume per unit cell is approximately 41.7%.

Compound **3** crystallizes in the monoclinic space group  $P2_1/n$  and also adopts a pillared-bilayer structure. The asymmetric unit of **3** contains two  $\text{Zn}^{\text{II}}$  ions, one tpim ligand, two  $\text{aip}^{2-}$  ligands, two and a half guest DMF molecules, and two guest water molecules. Both  $\text{Zn}(1)$  and  $\text{Zn}(2)$  centres adopt distorted tetrahedral coordination environments (Fig. 3a). Each  $\text{Zn}^{\text{II}}$  ion is bridged by an  $\text{aip}^{2-}$  ligand to produce a 2D layer with the same coordination mode as that in **1** and **2**. Interestingly, the tpim ligand possesses three pyridine groups but only two of these serve as pillars to interlink a pair of layers to create 1D channels inside the bilayers (Fig. 3b). 1D rhombic-shaped channels can be observed along the  $b$  axis with dimensions of  $5.1 \times 9.8 \text{ \AA}^2$  (Fig. 3c). The  $\text{Zn}^{\text{II}} \cdots \text{Zn}^{\text{II}}$  separation distance across the tpim bridge is  $13.6(9) \text{ \AA}$ . The channels were occupied by guest DMF and water molecules. Analysis using PLATON software indicated that the extra-framework volume per unit cell is approximately 33.9%.





The diagram illustrates the construction of a 3D crystal lattice from 1D and 2D building blocks. It shows three examples of how 1D or 2D structures are combined to form a 3D lattice:

- Top:** A 3D molecular structure (a central carbon atom bonded to three oxygen atoms, each with a red sphere) is shown next to an equals sign and a simplified 3D representation of the same structure (a central orange sphere bonded to three purple spheres).
- Middle:** Two 1D chains of molecules (labeled 1 and 2) are shown next to an equals sign and a single 1D chain. This chain is then shown next to an arrow pointing to a 3D lattice structure, where the 1D chains are stacked and connected to form a 3D framework.
- Bottom:** A 2D molecular structure (labeled 3) is shown next to an equals sign and a single 2D layer. This layer is then shown next to an arrow pointing to a 3D lattice structure, where the 2D layers are stacked and connected to form a 3D framework.

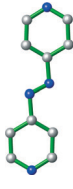
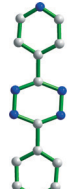
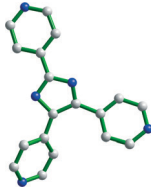
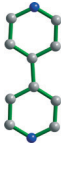
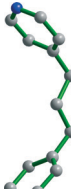
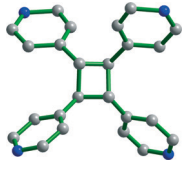
**Fig. 4** A simplified view of the pillared-bilayer networks of 1–3.

Although the constructions of the pillared-bilayer MOFs in 1–3 are similar, based on the 2D lamina, it should be noted that there are structural differences between them. The  $\beta$  angles of the monoclinic cell of 1–3 are  $106.4(3)^\circ$ ,  $102.3(2)^\circ$ , and  $99.7(13)^\circ$ , respectively, with the reflection corresponding to an adjacent 2D layer bridged by the pillar ligands. In the cases of 1 and 2, we attempted to increase the length of the pillar ligands to increase the porosity of the frameworks. In compound 3, the uncoordinated pyridyl group of the tpim ligand caused a reduction in the inner cavity space, but large one-dimensional channels were formed. Furthermore, the pillaring ligands azpy, dipytz, and ptim successfully modulate the size and shape of the channel spaces of the resulting arrays of networks. On the basis of the structures of 1 and 2, two linear-shaped pillaring ligands (azpy and dipytz) provided  $\text{--N=N--}$  and tetrazine functional group decorated channel surfaces, respectively. It is noteworthy that in the case of compound 3, some significant features are observed such as (1) only two pyridyl groups of the tpim ligand are coordinated to the metal centres that support the  $[\text{Zn}(\text{aip})]_n$  layers, therefore, the third pyridyl group resembles a pendent arm and the imidazole moiety serves as a functional decoration of the channel wall, and (2) the tpim ligand is able to participate in strong  $\pi$ – $\pi$  interactions between the regularly arranged tpim pillars, thus enhancing the rigidity of the resulting pillared-bilayer host of 3 (Fig. S8†). Pillared-bilayer MOFs are rare in the literature and several are listed in Table 3. More importantly, the results of this study revealed that the 2D pillared-bilayer structures can be systematically synthesized and allow open frameworks with tunable pore sizes and shapes to be produced when appropriate functionalized pillar ligands are employed.

### Thermogravimetric analyses

Thermogravimetric analyses (TGA) of **1** revealed a weight loss of 4.2% (calculated 3.7%) in the range of 25–40 °C, which

**Table 3** The modulation of the pillar-functionalized bilayer array networks

Compound	1	2	3	Ref. 6a	Ref. 6a	Ref. 5c
Pillar ligand						
Channel sizes ( $\text{\AA}^2$ )	$4.1 \times 10.1$ $3.1 \times 4.3$	$4.1 \times 11.1$ $4.3 \times 4.4$	$5.1 \times 9.8$	$3.5 \times 6.7$ $2.1 \times 4.1$	$3.9 \times 7.8$	×
Solvent accessible area	35.7%	41.7%	33.9%	20.7%	25.5%	7.8%

corresponds to the loss of two  $\text{H}_2\text{O}$  molecules. A second weight loss of 17.5% (calculated 17.6%) was then observed in the range of 40–158 °C, corresponding to the release of two DMF molecules, and the entire structure begins to decompose, eventually collapsing at 300 °C. The TGA curve of **2** revealed a weight loss of 8.6% (calculated 7.3%) during the first step from 25 to 88 °C, corresponding to the loss of two guest water molecules and a methanol molecule, and a second weight loss of 8.2% (calculated 9.6%) was observed in the range of 88–158 °C, corresponding to the release of a DMF molecule. The framework began to decompose with a continuous weight loss at temperatures over 290 °C, which can be attributed to the loss of the coordinating ligands. The TGA profile of **3** revealed a weight loss of 19.8% (calculated 21.6%) in the range of 25–190 °C, which can be attributed to the loss of the guest water and DMF molecules (Fig. S9†). The framework was stable up to 420 °C.

#### Powder X-ray diffraction analyses

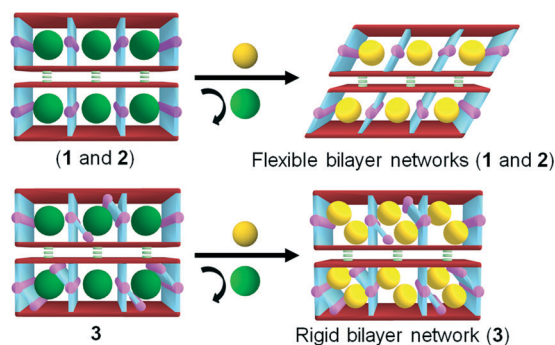
Powder X-ray diffraction (PXRD) were carried out to confirm the phase purity of **1–3** as well as their stability upon undergoing solvent-exchange processes. The results showed that all peaks were in good agreement with the corresponding simulated patterns (Fig. S10–S12†). Furthermore, the patterns of the methanol-exchanged samples indicated that an acceptable degree of crystallinity was maintained (Fig. S13–S15†). The PXRD patterns of methanol-exchanged **1** and **2** were slightly different from those of the as-synthesized samples, suggesting the possibility that **1** and **2** are structurally flexible. For compound **3**, the peaks for the methanol-exchanged sample were slightly shifted from the simulated peak positions but the crystallinity was maintained, which indicated that the compound is more rigid and retains its stability after guest exchange. A schematic representation of the structural transformation upon guest exchange is shown in Scheme 2.<sup>14</sup>

#### Gas adsorption studies

In order to explore the gas sorption properties of the pillared-bilayer frameworks, freshly prepared samples were immersed in methanol for 2 days at room temperature to allow the solvents to be exchanged. The guest-exchanged compounds were

confirmed by the disappearance of a strong DMF  $\text{C}=\text{O}$  stretching peak at  $1668\text{ cm}^{-1}$  in the IR spectrum (Fig. S17†). All of these compounds were desolvated at 120 °C overnight under vacuum. The results were verified by TGA analyses, which showed that the guest DMF molecules in **1–3** had been completely exchanged and removed. Gas sorption experiments of compounds **1–3** were carried out under nitrogen, hydrogen, and carbon dioxide atmospheres, respectively, to investigate their pore properties and gas storage capabilities. The activated samples, after removal of methanol, remained stable and no appreciable amount of mass was lost until they undergo decomposition (Fig. S16†). The results indicated that activated compounds **1–3** adsorbed only a minor amount of  $\text{N}_2$  at 77 K and 1 atm (Fig. S18†).  $\text{N}_2$  molecules did not diffuse into the channels in compounds **1–3**, which may be due to possible framework contraction and the absence of appropriate intermolecular interactions at low temperature.

The  $\text{CO}_2$  adsorption isotherms of **1–3** at 195 K showed type I adsorption behavior, which is characteristic of microporous materials (Fig. 5). To our surprise, adsorption measurements showed that the total amount of  $\text{CO}_2$  taken up by **1–3** was 53.1, 89.9, and  $121.7\text{ cm}^3\text{ g}^{-1}$ , respectively, with apparent Brunauer–Emmett–Teller (BET) surface areas of 132, 248, and  $317\text{ m}^2\text{ g}^{-1}$  (Langmuir surface areas of 239, 400, and  $539\text{ m}^2\text{ g}^{-1}$ ). Significantly, compound **3** showed a larger  $\text{CO}_2$  adsorption capacity than compounds **1** and **2**. In addition, the  $\text{CO}_2$  adsorption value for **3** was higher than that



**Scheme 2** Schematic representation of the structural transformation of the 2D pillared-bilayer networks with 1D channels upon undergoing a solvent-exchange process.

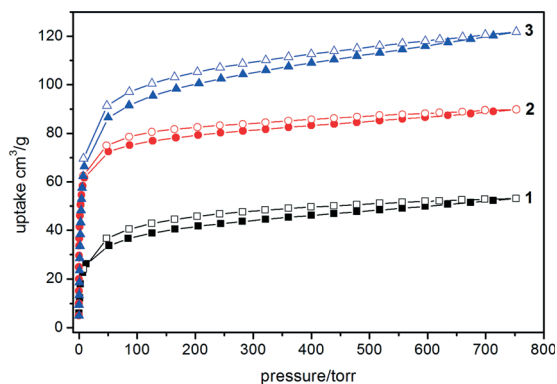


Fig. 5 CO<sub>2</sub> adsorption isotherms of 1–3 at 195 K.

for many previously reported 2D porous MOFs.<sup>15</sup> In the case of 1 and 2, the smaller pore volume as well as the lesser void space, as calculated by PLATON, was also reflected in the lower uptake of CO<sub>2</sub>. This can be attributed to the decreased length of the linear-shaped pillar linkers as well as the flexible nature of the pillared-bilayer structure. In compound 3,  $\pi$ - $\pi$  stacking interactions of the dangling arm of the ptm linker significantly strengthened the rigidity of the pillared-bilayer network. Furthermore, the imidazole moiety as well as the uncoordinated pyridyl group of the pillar ligand in the channels of compound 3 also facilitated interactions with respect to CO<sub>2</sub> molecules.<sup>16</sup>

The H<sub>2</sub> adsorption isotherms of 1–3 were probed at 77 K. The maximum amounts of H<sub>2</sub> taken up were 14.3, 6.5, and 55.7 m<sup>3</sup> g<sup>-1</sup> for 1–3, respectively. Interestingly, compound 3 showed the greatest H<sub>2</sub> uptake as compared to compounds 1 and 2, and displayed a reversible type I adsorption isotherm in this series (Fig. 6). The sorption isotherm of 3 also displays a small hysteresis, which revealed strong interactions between H<sub>2</sub> and the host framework. On the contrary, the networks of 1 and 2 were less effective for hydrogen adsorption, possibly due to framework contraction and the absence of appropriate intermolecular interactions at low temperature.

To better understand the adsorption properties of compounds 1–3, the heats of adsorption ( $Q_{st}$ ) of the CO<sub>2</sub>

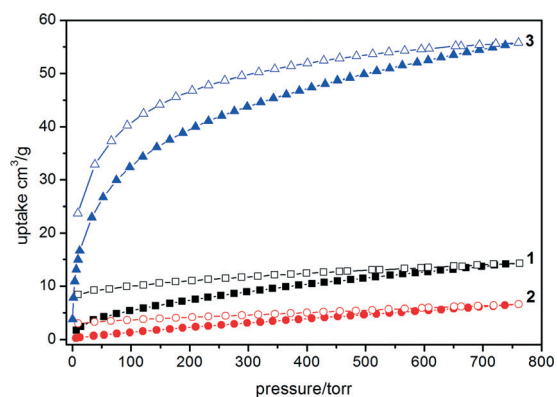


Fig. 6 H<sub>2</sub> adsorption isotherms of 1–3 at 77 K.

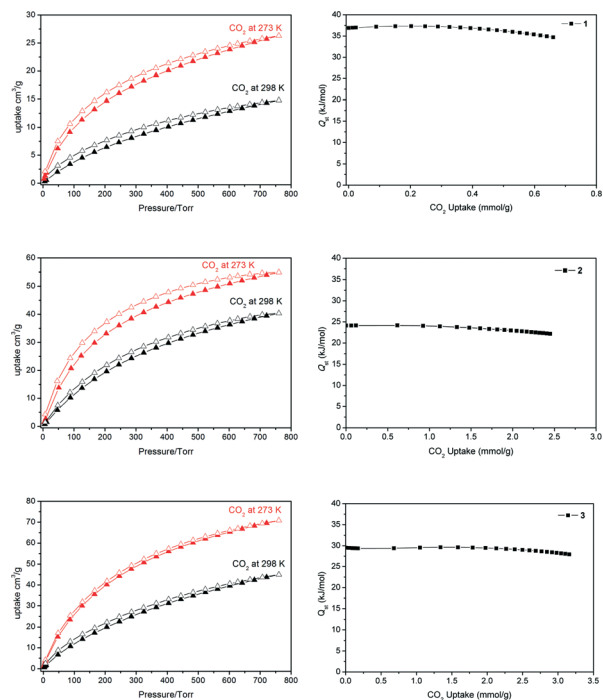


Fig. 7 CO<sub>2</sub> adsorption isotherms at 273 K and 298 K (left) and the isosteric heats ( $Q_{st}$ ) of CO<sub>2</sub> adsorption (right) for 1–3.

adsorption isotherms were calculated at 273 K and 298 K by using both the virial fitting method and the Clausius–Clapeyron equation.<sup>17</sup> As shown in Fig. 7, at zero loading, the  $Q_{st}$  values ( $-\Delta H$ ) for compounds 1–3 were determined to be 36.8, 24.1 and 29.5 kJ mol<sup>-1</sup>, respectively, showing steady retention at higher coverages. The  $Q_{st}$  value for 1 was the highest compared to reported pervious microporous 2D MOFs, in which the pore surfaces are decorated with  $-N=N-$  functional groups (20 kJ mol<sup>-1</sup>).<sup>18</sup> Interestingly, compound 1 possessed a greater  $Q_{st}$  value than compound 2, suggesting that the narrow pore size and pore surface (decorated with a  $-N=N-$  group) facilitate the optimization of the CO<sub>2</sub>-framework and adsorbate-adsorbent interactions within the 1D channels.<sup>19</sup> On the other hand, compound 3 showed higher CO<sub>2</sub> and H<sub>2</sub> uptake capacities than compounds 1 and 2, indicating that the rigidity and stability of the pillared-bilayer networks are important factors for effective gas adsorption. In short, by modulating the pillar-functionalized pores in the series of compounds 1–3, it was possible to successfully tune the porosity, functionality, rigidity (flexibility) and selectivity of such materials for gas adsorption.

## Conclusions

We systemically synthesized three pillared-bilayer Zn(II)-organic frameworks, in which 2D layers were connected by functionalized pillared ligands. The resulting MOFs show tunable structures, as their pore size and rigidity (flexibility) could be controlled by adjusting the length, shape and functionality of the pillared ligands. Their structural characteristics allow



these pillared-bilayer MOFs to serve as excellent models for studies of gas adsorption properties.

## Acknowledgements

We are grateful to Academia Sinica, National Central University and the Ministry of Science and Technology of Taiwan for financial support.

## Notes and references

- (a) S. Kitagawa, R. Kitaura and S. I. Noro, *Angew. Chem., Int. Ed.*, 2004, **43**, 2334; (b) T. T. Luo, H. L. Tsai, S. L. Yang, Y. H. Liu, R. D. Yadav, C. C. Su, C. H. Ueng, L. G. Lin and K. L. Lu, *Angew. Chem., Int. Ed.*, 2005, **44**, 6063; (c) Y. Z. Zheng, M. L. Tong, W. Xue, W. X. Zhang, X. M. Chen, F. Grandjean and G. J. Long, *Angew. Chem., Int. Ed.*, 2007, **46**, 6076; (d) M. O'Keeffe and O. M. Yaghi, *Chem. Rev.*, 2012, **112**, 675; (e) X. S. Wang, M. Chrzanowski, W. Y. Gao, L. Wojtas, Y. S. Chen, M. J. Zaworotko and S. Ma, *Chem. Sci.*, 2012, **3**, 2823.
- (a) R. E. Morris and P. S. Wheatley, *Angew. Chem., Int. Ed.*, 2008, **47**, 4966; (b) L. J. Murray, M. Dincă and J. R. Long, *Chem. Soc. Rev.*, 2009, **38**, 1294; (c) A. Phan, C. J. Doonan, F. J. Uribe-Romo, C. B. Knobler, M. O'Keeffe and O. M. Yaghi, *Acc. Chem. Res.*, 2010, **43**, 58; (d) J. R. Li, J. Sculley and H. C. Zhou, *Chem. Rev.*, 2012, **112**, 869; (e) Y. Yan, S. Yang, A. J. Blake and M. Schröder, *Acc. Chem. Res.*, 2014, **47**, 296.
- (a) M. Zhao, S. Ou and C. D. Wu, *Acc. Chem. Res.*, 2014, **47**, 1199; (b) M. Yoon, R. Srirambalaji and K. Kim, *Chem. Rev.*, 2012, **112**, 1196; (c) S. Yang, L. F. Liu, J. L. Sun, K. M. Thomas, A. J. Davies, M. W. George, A. J. Blake, A. H. Hill, A. N. Fitch, C. C. Tang and M. Schröder, *J. Am. Chem. Soc.*, 2013, **135**, 4954.
- (a) M. D. Allendorf, C. A. Bauer, R. K. Bhakta and R. J. T. Houk, *Chem. Soc. Rev.*, 2009, **38**, 1330; (b) L. E. Kreno, K. Leong, O. K. Farha, M. Allendorf, R. P. V. Duyne and J. T. Hupp, *Chem. Rev.*, 2012, **112**, 1105.
- (a) H. J. Choi and M. P. Suh, *J. Am. Chem. Soc.*, 2004, **126**, 15844; (b) K. L. Gurunatha, S. Mohapatra, P. A. Suchetan and T. K. Maji, *Cryst. Growth Des.*, 2009, **9**, 3844; (c) M. Dai, W. Y. Yan, Z. G. Ren, H. F. Wang, W. J. Gong, F. L. Li, X. Zhao, H. X. Li and J. P. Lang, *CrystEngComm*, 2012, **14**, 6230; (d) Z. Yin, Y. L. Zhou, M. H. Zeng and M. Kurmoo, *Dalton Trans.*, 2015, **44**, 5258.
- (a) K. O. Kongshaug and H. Fjellvåg, *Inorg. Chem.*, 2006, **45**, 2424; (b) J. T. Shi, C. S. Zhou, Y. L. Liu, Z. G. Fang, R. L. Zhao, L. L. Xu and K. F. Yue, *Z. Anorg. Allg. Chem.*, 2013, **639**, 187; (c) R. Haldar and T. K. Maji, *CrystEngComm*, 2013, **15**, 9276; (d) X. L. Wang, F. F. Sui, H. Y. Lin, J. W. Zhang and G. C. Liu, *Cryst. Growth Des.*, 2014, **14**, 3438.
- (a) T. K. Maji, K. Uemura, H. C. Chang, R. Matsuda and S. Kitagawa, *Angew. Chem., Int. Ed.*, 2004, **43**, 3269; (b) H. Ren, T. Y. Song, J. N. Xu, S. B. Jing, Y. Yu, P. Zhang and L. R. Zhang, *Cryst. Growth Des.*, 2009, **9**, 105; (c) Z. Chang, D. S. Zhang, Q. Chen, R. F. Li, T. L. Hu and X. H. Bu, *Inorg. Chem.*, 2011, **50**, 7555; (d) S. Henke, A. Schneemann, A. Wütscher and R. A. Fischer, *J. Am. Chem. Soc.*, 2012, **134**, 9464; (e) J. T. Culp, C. Madden, K. Kauffman, F. Shi and C. Matranga, *Inorg. Chem.*, 2013, **52**, 4205; (f) C. H. Lee, J. Y. Wu, G. H. Lee, S. M. Peng, J. C. Jiang and K. L. Lu, *Cryst. Growth Des.*, 2014, **14**, 5608; (g) X. L. Zhao, F. L. Liu, L. L. Zhang, D. Sun, R. M. Wang, Z. F. Ju, D. Q. Yuan and D. F. Sun, *Chem. – Eur. J.*, 2014, **20**, 649.
- J. P. Launay, M. Tournel-Pagis, J. F. Lipskier, V. Marvaud and C. Joachim, *Inorg. Chem.*, 1991, **30**, 1033.
- P. H. Dinolfo, M. E. Williams, C. L. Stern and J. T. Hupp, *J. Am. Chem. Soc.*, 2004, **126**, 12989.
- M. V. Proskurnina, N. A. Lozinskaya, S. E. Tkachenko and N. S. Zefirov, *Russ. J. Org. Chem.*, 2002, **38**, 1149.
- G. M. Sheldrick, A Short History of SHELX, *Acta Crystallogr., Sect. A: Found. Crystallogr.*, 2008, **64**, 112.
- A. L. Spek, *J. Appl. Crystallogr.*, 2003, **36**, 7.
- M. Dai, W. Y. Yan, Z. G. Ren, H. F. Wang, W. J. Gong, F. L. Li, X. Zhao, H. X. Li and J. P. Lang, *CrystEngComm*, 2012, **14**, 6230.
- (a) S. Kitagawa and K. Uemura, *Chem. Soc. Rev.*, 2005, **34**, 109; (b) Y. Kubota, M. Takata, R. Matsuda, R. Kitaura, S. Kitagawa and T. C. Kobayashi, *Angew. Chem., Int. Ed.*, 2006, **45**, 4932; (c) A. Kondo, H. Kajiro, H. Noguchi, L. Carlucci, D. M. Proserpio, G. Ciani, K. Kato, M. Takata, H. Seki, M. Sakamoto, Y. Hattori, F. Okino, K. Maeda, T. Ohba, K. Kaneko and H. Kanoh, *J. Am. Chem. Soc.*, 2011, **133**, 10512; (d) Z. H. Xuan, D. S. Zhang, Z. Chang, T. L. Hu and X. H. Bu, *Inorg. Chem.*, 2014, **53**, 8985.
- (a) T. K. Maji, G. Mostafa, R. Matsuda and S. Kitagawa, *J. Am. Chem. Soc.*, 2005, **127**, 17152; (b) P. Kanoo, G. Mostafa, R. Matsuda, S. Kitagawa and T. K. Maji, *Chem. Commun.*, 2011, **47**, 8106; (c) S. Parshamoni, S. Sanda, H. S. Jena and S. Konar, *Dalton Trans.*, 2014, **43**, 7191.
- (a) J. B. Lin, W. Xue, J. P. Zhang and X. M. Chen, *Chem. Commun.*, 2011, **47**, 926; (b) W. Y. Gao, W. Yan, R. Cai, K. Williams, A. Salas, L. Wojtas, X. Shi and S. Ma, *Chem. Commun.*, 2012, **48**, 8898; (c) P. Z. Li, X. J. Wang, R. H. D. Tan, Q. Zhang, R. Q. Zou and Y. L. Zhao, *RSC Adv.*, 2013, **3**, 15566.
- J. L. C. Rowsell and O. M. Yaghi, *J. Am. Chem. Soc.*, 2006, **128**, 1304.
- (a) P. Kanoo, A. C. Ghosh, S. T. Cyriac and T. K. Maji, *Chem. – Eur. J.*, 2012, **18**, 237; (b) N. Sikdar, A. Hazra and T. K. Maji, *Inorg. Chem.*, 2014, **53**, 5993.
- (a) C. M. Nagaraja, R. Haldar, T. K. Maji and C. N. R. Rao, *Cryst. Growth Des.*, 2012, **12**, 975; (b) B. Bhattacharya, R. Dey, P. Pachfule, R. Banerjee and D. Ghoshal, *Cryst. Growth Des.*, 2013, **13**, 731; (c) B. Bhattacharya, D. Saha, D. K. Maity, R. Dey and D. Ghoshal, *CrystEngComm*, 2014, **16**, 4783.